CHEMISTRY OF MATERIALS
Cite This: Chem. Mater. XXXX, XXX, XXX−XXX
Article
pubs.acs.org/cm

Understanding the Electrochemical Properties of Naphthalene Diimide: Implication for Stable and High-Rate Lithium-Ion Battery Electrodes

Yang Shi,[†] Hanmei Tang,[†] Shengli Jiang,[†] Laure V. Kayser,[†] Mingqian Li,[†] Fang Liu,[§] Fei Ji,[†] Darren J. Lipomi,[†] Shyue Ping Ong,[†] and Zheng Chen*[,†,‡]

[†]Department of NanoEngineering and [‡]Program of Materials Science and Engineering, University of California, San Diego, La Jolla, California 92093, United States

[§]Department of Chemical and Biomolecular Engineering, University of California, Los Angeles, Los Angeles, California 90095, United States

Supporting Information

ABSTRACT: Redox-active organic molecules have attracted much attention as alternatives to transition-metal-based electrodes for lithium-ion batteries due to their low cost and large abundance. However, the relatively low cycling stability still prevents some of the most promising molecules to be used as lithium-ion electrodes. Herein, we used 1,4,5,8-naphthalene diimide (NDI) as a model molecule to systematically investigate its intrinsic electrochemical property, including its electrolyte compatibility, maximum capacity, cycling stability, and rate capability in different organic electrolytes. Extensive physicochemical characterization, electrochemical measurement, and density function theory (DFT) calculation together show that the electrode−electrolyte interaction is the key factor determining its specific capacity and cycling stability. With a proper selection of electrolytes, NDI molecule, which was considered to be not stable for lithium storage, can achieve near theoretical capacity (based on two-electron reaction), very high rate capability, and high cycling stability. This study suggests the importance of understanding the fundamental electrode−electrolyte interactions in designing high-performance organic electrodes.

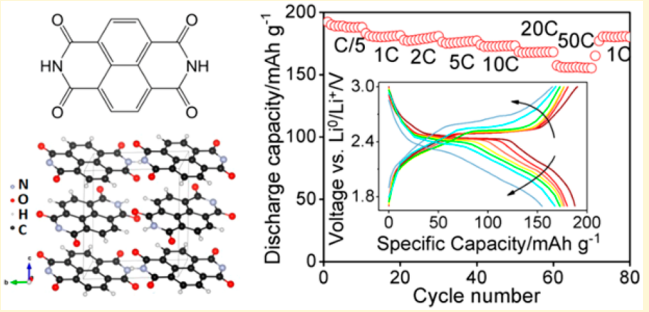

INTRODUCTION

Today's lithium-ion battery (LIB) technology heavily relies on expensive transition metal (e.g., cobalt, nickel, manganese) oxides, which starts to draw significant concern on the resource shortage and environmental issues.[1−4] As the demand for high-performance and low-cost batteries continues to grow, sustainable, cost-effective, and environmentally benign electrode materials need to be developed. In this context, redox-active organic molecules (small molecules and polymers) have attracted much attention as alternatives to transition-metal-based electrodes due to their low cost, low toxicity, and abundancy.[5−8] Typical redox-active materials include quinones, anhydrides, and imides which can bind and store cations through commonly recognized enolization mechanism.[9,10] Some of them have shown very high charge storage capacity (up to 400 mAh/g) in either aprotic or aqueous electrolytes, making them promising for high-energy lithium-ion electrodes.[11] However, some barriers still prevent the practical use of these materials. One critical issue is their relative low cycling stability due to undesired dissolution in the electrolytes.[12,13] The development of rigid molecular structures,[14−16] formation of organic salts,[17,18] and incorporation of redox-active groups into the insoluble polymer backbone[19,20] have been considered as potential strategies to reduce their solubility in electrolyte. While the structure stability can be improved to a certain extent, chemical interactions between redox active groups and electrolyte still limit the electrode cycling stability. In addition, these strategies often reduce the specific capacity (due to increased inactive mass) and require a complicated synthesis. To date, there are only a limited number of organic electrodes that can be as stable as their inorganic counterparts (e.g., less than 20% of capacity loss for 300 charge/discharge cycles).

Among a large number of derivatives of aromatic diimides, 1,4,5,8-naphthalene diimide (NDI) (also known as naphthalene carbodiimides), a n-type molecule often used in organic electronics, photovoltaic devices, and sensors, has been recently considered as a potential lithium-ion electrode due to its small molecular weight, high electron affinity, and good charge carrier mobility.[21−23] Its carbonyl groups can receive electrons and bind Li^+ to form lithium enolate, and Li^+ can be disassociated in

Received: March 29, 2018
Revised: April 27, 2018
Published: April 27, 2018

DOI: 10.1021/acs.chemmater.8b01304
Chem. Mater. XXXX, XXX, XXX−XXX

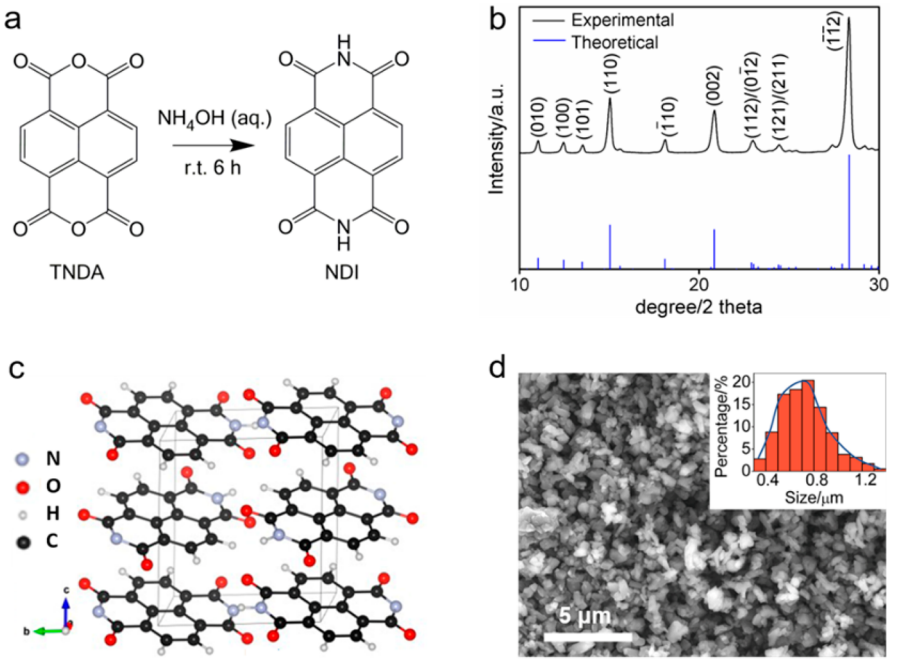

Figure 1. (a) Chemical structures of NTDA and NDI, (b) experimental and theoretical XRD patterns of NDI molecules, (c) crystal structures of NDI, and (d) SEM images of NDI with the inset showing the particles size distribution.

the reverse oxidation/reduction process. A reasonably high specific capacity of ~200 mAh/g can be expected based on two-electron reaction (2 Li per NDI molecule). The rigidity of the pyrene in NDI molecules can restrict their dissolution in organic electrolytes, suggesting their good cycling stability. However, previously investigated NDI (and their derivatives) electrodes often showed low discharge capacity of 140−170 mAh g^{-1} and/or a poor cycling stability (capacity decreased to 80−120 mAh g^{-1} after 20 cycles).[10,24] These observations indicate that fundamental understanding of the electrochemical nature of NDI molecules remains needed.

In this work, we used NDI as a model material to perform a systematic study to fully understand its intrinsic electrochemical property, including its electrolyte compatibility, maximum capacity, cycling stability, rate capability, and structure evolution during discharge/charge. Extensive physicochemical characterization, electrochemical measurement, and density function theory (DFT) calculation together show that the electrode−electrolyte interaction is the key factor determining its specific capacity and cycling stability. With a proper selection of electrolytes, NDI electrode can achieve near theoretical lithium storage capacity, long cycle life (96% capacity retention at a rate of 1 C after 400 cycles), and very high rate capability (82% of the capacity even at a rate of 50 C with an 81% capacity retention after 2000 cycles). This study suggests the importance of understanding the fundamental electrode−electrolyte interactions in designing high-performance organic electrodes.

EXPERIMENTAL SECTION

Synthesis and Characterization of NDI. NDI was synthesized by dissolving 1,4,5,8-naphthalenetetracarboxylic dianhydride (12.5 g, Sigma-Aldrich) in an aqueous solution of ammonium hydroxide (625 mL, 28 wt %, Alfa Aesar). The mixture was stirred at room temperature for 6 h under nitrogen. NDI precipitated as a pale yellow solid which was recovered by centrifugation, washed with DI water, and dried under vacuum. Elemental analysis found the C and N content in the sample to be 62.85% and 10.40% in weight, respectively, which is close to the calculated values: 63.17% for C and 10.52% for N. ^{1}H NMR was performed on a Varian Mercury 400 MHz spectrometer in D_2SO_4 using 4,4-dimethyl-4-silapentane-1-sulfonic acid (DSS) as an internal standard: δ 8.53 ppm (s, 4H, Ar). The NDI powder was examined by X-ray powder diffraction (XRD) employing Cu Kα radiation with a Bruker D2 Phaser. The morphology of NDI powders was observed by an ultrahigh resolution scanning electron microscope (UHR SEM, FEI XL30). The particle size distribution was analyzed with a Nano Measurer.

NDI Electrodes Fabrication and Coin Cell Assembly. NDI was first dispersed in tetrahydrofuran, followed by sonication to get a uniform dispersion. Then Ketjen black was added to the dispersion and sonicated, and the tetrahydrofuran was evaporated during stirring. Ketjen black−NDI composite is mixed with Super P and poly(vinylidene fluoride) (PVDF) using a mortar and pestle, followed by adding NMP to obtain a uniform slurry. The mass ratio of NDI, Ketjen black, Super P, and PVDF is 0.64:0.16:0.1:0.1. The carbon paper (Fuel Cell store) was cut into disks with a diameter of 12 mm, and the slurry was drop-casted on the carbon paper, followed by vacuum drying at 80 °C for 6 h. The mass loading of typical NDI electrodes is 1−2 mg cm^{-2}. To fabricate high mass loading NDI, the Ketjen black−NDI composite was mixed with Super P and PTFE suspension in ethanol, forming a doughlike texture. The mixture was kneaded and folded, followed by passing through the rolling mill. The compressed mixture formed a free-standing sheet, which was cut into disk electrodes with a diameter of 12 mm. The resulted NDI mass loading is about 20 mg cm^{-2}.

The 2032-type coin cells were assembled with Li metal disc (thickness 1.1 mm) as anode, 1 M LiTFSI in dioxolane, and dimethoxyethane (DOL:DME 1:1 vol), 1 M $LiClO_4$ in DOL:DME (1:1 vol), 1 M LiTFSI in EC:DEC 1:1 vol, or 1 M $LiPF_6$ in EC:DEC 1:1 vol as the electrolyte and trilayer membrane (Celgard 2320) as the separator. The cycling stability and rate capability were tested using a Land battery testing system.

Electrochemical Impedance Spectroscopy (EIS) and X-ray Photoelectron Spectroscopy (XPS). EIS tests were performed on the coin cells assembled with different electrolyte at discharged state in the frequency range of 10^6 to 10^{-3} Hz with a signal amplitude of 10 mV by a Metrohm Autolab potentiostat. The electrodes after 200 cycles were analyzed using XPS (AXIS Ultra DLD) with Al Kα

DOI: 10.1021/acs.chemmater.8b01304
Chem. Mater. XXXX, XXX, XXX−XXX

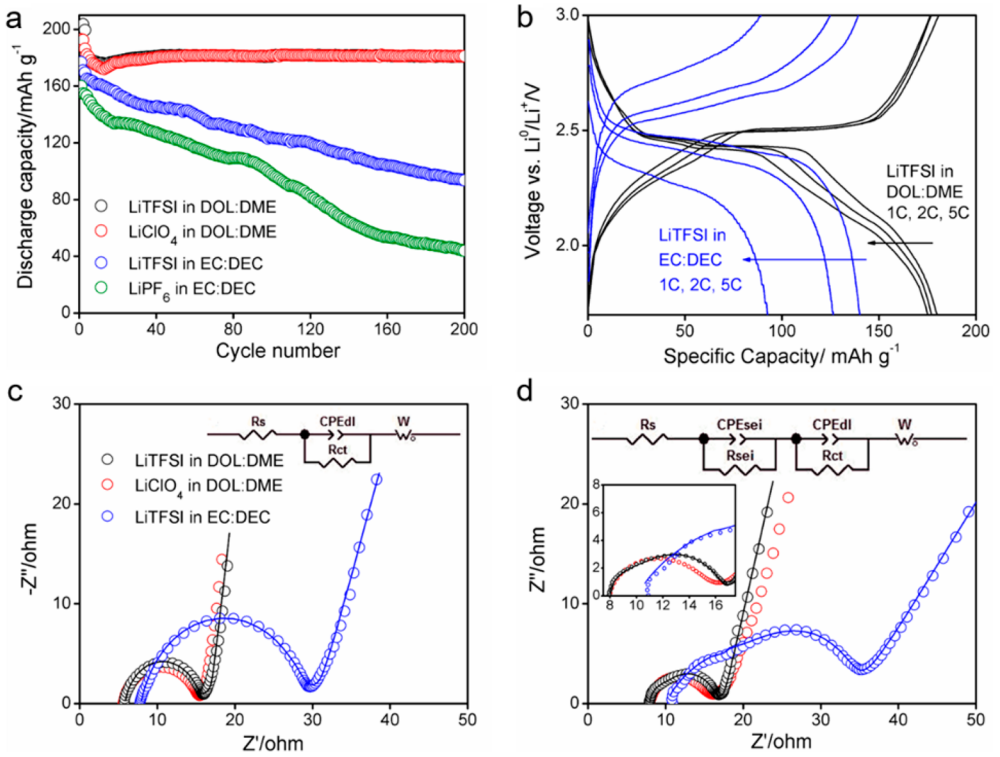

Figure 2. (a) Cycling performance of NDI electrodes in different electrolytes. (b) Voltage profiles of NDI electrodes at 1C, 2C, and 5C in the ether- and carbonate-based electrolytes. (c) Nyquist plots of fresh NDI cells. Scatter: experimental data; line: fitted plot. The inset shows the equivalent circuit. (d) Nyquist plots of cells after 100 cycles at 1C. The insets show the equivalent circuit and the enlarged plot in the high-frequency region.

radiation. The samples were transferred under inert atmosphere to the XPS testing chamber prior to analysis.

***Ex-Situ* XRD and *ex-Situ* FT-IR.** Because of the strong graphite peaks in XRD patterns for electrodes on carbon paper, NDI electrodes with the same composition as stated previously on Al substrate were fabricated. NMP was added to the mixture to form uniform slurry, which was casted on Al substrate with doctor blade. The mass loading of NDI is about 1 mg/cm^2. Coin cells were assembled in the same procedure as stated previously, with 1 M LiTFSI in DOL:DME (1:1 vol) as an electrolyte. The cells were discharged and charged at a current of 20 mA g^{-1} to minimize the polarization and then disassembled at different voltages. The cathodes were thoroughly rinsed with DOL:DME (1:1 vol), and the electrode material was removed from the Al current collector. The harvested material was sealed in a capillary tube with a diameter of 500 μm in the glovebox. XRD data were collected on a Bruker K3 Kappa diffractometer coupled to a Bruker Microstar rotating anode generator with Cu Kα radiation (λ = 1.541 78 Å), using a Bruker Vantec 500 area detector at the UCSD X-ray Crystallography Facility. Diffraction images were processed in DIFFRAC.EVA to give 2D X-ray diffraction plots. Fourier transform infrared spectroscopy (FT-IR) measurements were performed on the electrodes prepared in the same procedure, using a Bruker ALPHA FTIR spectrometer.

RESULTS AND DISCUSSION

Synthesis and Characterization. NDI was synthesized according to the method reported before.[25] 1,4,5,8-Naphthalenetetracarboxylic dianhydride (NTDA) (Figure 1a) was dissolved in an aqueous solution of ammonium hydroxide (30 wt %) and stirred at room temperature for 6 h under nitrogen. NDI precipitated as a pale yellow product which was recovered by centrifugation, washed with water, and dried under vacuum. Elemental analysis found the C and N content in the sample to be 62.85% and 10.40% in weight, respectively, which is close to the calculated values of 63.17% for C and 10.52% for N. The ^{1}H NMR spectrum of NDI in D_2SO_4 displays a single peak at δ = 8.53 ppm (s), characteristic of aromatic protons, further confirming the desired composition and purity. The crystal structure of NDI can be well indexed in their XRD patterns (Figure 1b) (full XRD pattern is displayed in Figure S1a). The experimental results match well with the theoretical patterns, revealing that NDI has a triclinic crystal structure with parallel layers (Figure 1c).[26] The (−1−12) plane is identified as the main plane for the layered structure (Figure S1) and has the highest peak intensity. The SEM images and the derived particle size distribution show that the synthesized NDI has particle sizes ranging from 0.3 to 1.4 μm (Figure 1d).

Electrolyte Compatibility. Since the literature shows inconsistent cycling stability of NDI in different electrolytes, we first explored the compatibility of NDI electrodes with different electrolytes. NDI powder was mixed with conductive carbon and PVDF to form a slurry which was casted on carbon paper substrates and dried under vacuum to form electrodes. Coin cells were made with different electrolytes, and Li metal was used as the anode. Each NDI electrode was cycled at C/5 (C = 200 mA g^{-1}) for the first three cycles and then 1C for the following cycles in the voltage range of 1.7−3 V (vs Li/Li$^+$). The tested electrolytes represented different classes of solvents and lithium salts, including 1 M lithium bis(trifluoromethanesulfonyl)imide (LITFSI) in dioxolane (DOL):dimethoxyethane (DME) (vol 1:1), 1 M $LiClO_4$ in DOL:DME, 1 M LiTFSI in ethylene carbonate (EC) and diethyl carbonate (DEC) (vol 1:1), and 1 M $LiPF_6$ in EC:DEC.

Figure 2a compares the cycling stability of NDI electrodes in different electrolytes. With the same DOL:DME solvent, the cycling performance of the electrodes with LiTFSI or $LiClO_4$ salts is equally good, showing no obvious capacity decay in 200 cycles. However, when the solvent is changed to EC:DEC, NDI

DOI: 10.1021/acs.chemmater.8b01304
Chem. Mater. XXXX, XXX, XXX−XXX

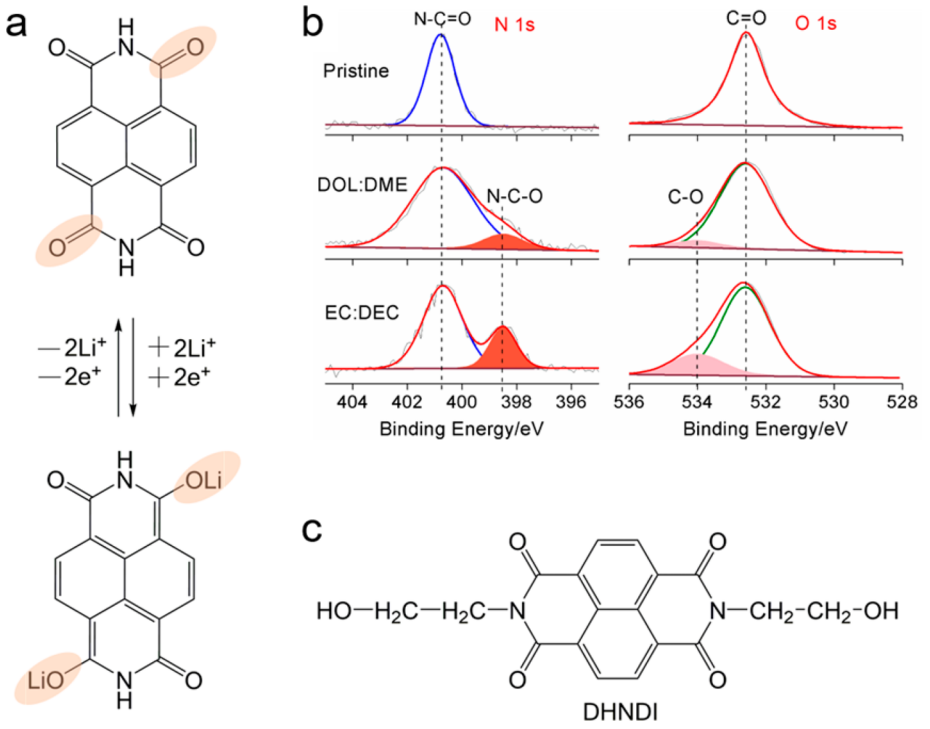

Figure 3. (a) Electrochemical lithiation and delithiation mechanism of NDI, (b) N 1s and O 1s XPS spectra of pristine and cycled electrodes in different electrolytes, and (c) possible reaction product of NDI and EC.

electrode shows faster capacity decay with either LiTFSI (45% decay) or $LiPF_6$ (75% decay) as the salt, suggesting undesired side reactions with these electrolytes. The voltage profiles of NDI electrodes at multiple rates in ether-based and carbonate-based electrolytes with LiTFSI as the salt are compared in Figure 2b. The NDI electrode in the ether-based electrolyte show little voltage drop at the beginning of discharging, while the voltage drop is much larger in the carbonate-based electrolyte. In addition, the NDI electrode has much lower average discharge voltage in the carbonate-based electrolyte than that in the ether-based electrolyte. The comparison of the voltage profiles indicates that the NDI electrode has significantly reduced polarization in ether-based electrolyte than that in carbonate-based electrolyte. To understand the stability characteristics, electrochemical impedance spectroscopy (EIS) was performed for the fresh cells and cells after 200 cycles (Figures 2c and 2d, respectively). The inset of Figures 2c and 2d shows the equivalent circuits to evaluate the resistance values of different components: R_s is the electrolyte resistance, R_{sei} the resistance of solid electrolyte interface (SEI), R_{ct} the charge transfer resistance, and W the Warburg impedance related to the diffusion of lithium ions.[27] Since the cells with LiTFSI and $LiClO_4$ salts show similar spectra, quantitative analysis of resistance values is performed on the cell with LiTFSI salt in ether-based electrolyte. The fresh cell has a R_s value of 5.98 Ω and R_{ct} value of 8.35 Ω. The resistance values are much lower than those of the fresh cell assembled with carbonate-based electrolyte with LiTFSI salt, which has a R_s value of 8.29 Ω and R_{ct} value of 18.69 Ω. After cycling, the R_s, R_{sei}, and R_{ct} values for the cell cycled in ether-based electrolyte are 7.93, 1.78, and 6.54 Ω, respectively. For the cell cycled in carbonate-based electrolyte, the R_s, R_{sei}, and R_{ct} values are 9.98, 15.48, and 8.81 Ω, respectively, higher than the resistance values in ether-based electrolyte. In both electrolytes the R_s values increase after cycling, while the R_{ct} values decrease after cycling. The reason for the decreased R_{ct} values in cycled cells might be that the fresh cells were not fully activated. The R_{SEI} of the cell cycled in carbonate-based electrolyte (15.48 Ω) is much higher than that cycled in ether-based electrolyte (1.78 Ω), which indicates the existence of a more resistive layer at the interface between the NDI electrode and the carbonate-based electrolyte.

We further investigated the potential reactions between NDI and different electrolytes. Figure 3a illustrates the mechanism of electrochemical lithiation reaction: one NDI molecule accommodates two Li^+ from two carbonyl groups, as suggested by previous studies.[10,24] Although there is a potential four-electron reaction mechanism resulting in the lithiation of the two remaining carbonyl groups, such attempts can result in serious structural damage and irreversible decomposition (will be discussed in further detail later). For the voltage window of our interest (1.7−3 V), the measured specific capacity (~200 mAh g^{-1}) at C/5 also matches two-electron reaction for NDI electrodes. X-ray photoelectron spectroscopy (XPS) was performed to analyze the surface reaction between NDI and solvent molecules. The XPS spectra of the pristine electrode and the electrodes at the charged state after 200 cycles in DOL:DME and EC:DEC electrolytes, both with LiTFSI as the salt are compared in Figure 3b. Since the carbonyl group is the redox site, N 1s and O 1s spectra of the three electrodes were obtained. In N 1s spectra, only the N−C═O peak at 400.7 eV is observed in the pristine electrode,[28] and after cycling, it generates N−C−O bond due to the incomplete delithiation as shown in the new peak at 398.5 eV. There are more N−C−O bonds in carbonate-based electrolyte than in ether-based electrolyte, which means that the polarization of NDI electrode cycled in the former is more severe than in the latter. In O 1s spectra, only the C═O peak at 532.5 eV is observed in pristine electrode, while C−O peak at 533.9 eV appears after cycling.[29−31] There are more C−O bonds in NDI electrode

DOI: 10.1021/acs.chemmater.8b01304
Chem. Mater. XXXX, XXX, XXX−XXX

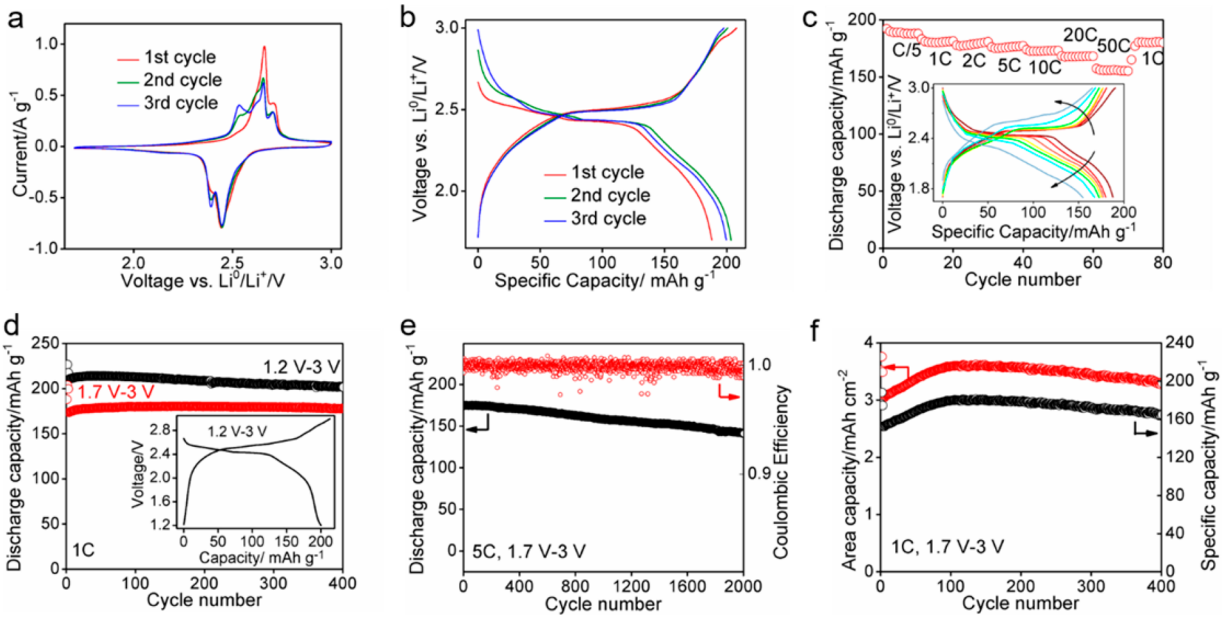

Figure 4. (a) CV plots of NDI electrodes in the first three cycles at a scan rate of 0.2 mV/s, (b) voltage−capacity profiles of NDI electrodes in the first three cycles at C/5, (c) rate capability of NDI, with the inset showing the capacity−voltage profiles at different rates, (d) cycling performance of NDI at 1C with cutoff voltages of 1.2 and 1.7 V, and the inset shows the capacity−voltage profile in the first cycle in the voltage range of 1.2−3 V, (d) cycling performance at 5 C in the voltage range of 1.7−3 V,and (f) cycling performance of high mass loading (20 mg cm^{-2}) electrodes at 1C in the voltage range of 1.7−3 V.

cycled in carbonate-based electrolyte than in ether-based electrolyte, which is consistent with the N 1s spectra. The results further support the larger polarization of the NDI electrode in carbonate-based electrolyte (Figure 2b).

There are two possible reasons for the rapid degradation of NDI electrodes in the carbonate-based electrolyte. First, NDI molecules may be soluble in the carbonate-based electrolytes, since the dissolution of the organic electrodes in carbonate solvent is commonly considered as a major problem that influences their electrochemical performance.[32] Second, NDI molecules can react with the carbonate-based electrolyte. To figure out whether NDI is soluble in the carbonate-based electrolyte, NDI electrodes were soaked in both DOL:DME and EC:DEC solvents. Different solvents including toluene, chloroform, chlorobenzene, hexane, dimethylformamide, and DMSO were tested to dissolve NDI, and it was found that DMSO has the highest solubility among them. Therefore, a dissolution test of NDI in DMSO was carried out in parallel with DOL:DME and EC:DEC as comparison to evaluate its solubility in the latter two solvents. No color change was observed in DOL:DME and EC:DEC after 7 days (Figure S2). In comparison, NDI in DMSO solution showed a yellow color. By measuring the weight of the undissolved NDI, the solubility of NDI in DMSO was found to be ~0.03 g/100 g, suggesting the low solubility of NDI even in DMSO. Therefore, we believe that the fast capacity decay of NDI electrodes in carbonate-based electrolyte is more likely caused by direct reaction between NDI and electrolyte solvent molecules. To test this hypothesis, pristine NDI powders were soaked in different solvents, and the FT-IR spectra of the soaked NDI were acquired. A sharp C−OH band can be observed for NDI powders soaked in EC:DEC, while not observed for NDI soaked in DEC or DOL:DME (Figure S3). Conversely, there was no extra peak for NDI soaked in DEC and DOL:DME. Therefore, we proposed a possible reaction process between NDI and EC molecules (decarboxylative N-alkylation) that generates the C−OH band. Similar reactions have been found in the hydroxyethylation of imides,[33] oxamides,[34−36] and adenines.[37−39] Similarly, the possible reaction product, dihydroxylethylnaphthalene diimide (DHNDI), is shown in Figure 3c. To confirm the product structure, the ^{1}H NMR spectrum of the mixture of NDI and EC was obtained (Figure S4), which supports the existence of DHNDI. Besides the signal of the aromatic protons of NDI at δ = 8.53 ppm, four new signals corresponding to the aromatic protons of the reaction product at 8.65 ppm, methylene signals at 4.66 and 5.23 ppm, and hydroxyl protons at 4.34 ppm are observed. ^{1}H NMR spectra of the mixture of NDI and DEC as well as NDI and DOL:DME were also obtained, and no extra signals were observed. Moreover, first-principles calculations also show that the above reaction is thermodynamically favored with a reaction energy of −0.35 eV (with details in the Supporting Information). This observation is also consistent with previous studies that a large group of aryl- and N-substituted NDI molecules show relatively fast capacity decay in carbonate-based electrolyte.[24] The newly formed DHNDI can exist as a resistive layer at the surface of the NDI electrode that hinders the Li^+ transport and/or electron transfer, which can explain the higher R_{SEI} value (Figure 2d) and larger polarization of the electrode (Figure 2b).

Electrochemical Characterization. From the above study, ether-based electrolytes are identified as the suitable electrolyte for NDI electrode. Therefore, to fully explore the electrochemical properties of NDI electrodes, extensive electrochemical characterization was performed based on 1 M LiTFSI in DOL:DME electrolyte. The cyclic voltammetry (CV) curve (Figure 4a) in the first cycle shows one pair of redox peaks with two small shoulders, on the negative side of the cathodic peak and positive side of the anodic peak. Starting from the second cycle, the cathodic peak evolves into two separate peaks, and the anodic peak evolves into three separate peaks gradually. After the third cycle, the peaks separation become stable, and

DOI: 10.1021/acs.chemmater.8b01304
Chem. Mater. XXXX, XXX, XXX−XXX

Table 1. Summary of High-Performance Organic Cathode Materials

material	capacity (mAh g^{-1})	cycling stability	voltage vs Li/Li^+ (V)	active mass loading (mg cm^{-2})
pyrene-4,5,9,10-tetraone[41]	231	83% after 500 cycles at 1C	two stages: 2.8 and 2.2	1.32
lumiflavine-SWNT[42]	204	99.7% after 100 cycles at 1C	2.5	
DBT/CMK-3[43]	400	83.9% after 100 cycles at 0.2C	2.5	
polyanthraquinone[44]	248	98.1% after 1000 cycles at 1C	2.14	1−2
Li_2PDHBQS[45]	240	90% after 1000 cycles at 2C	2.03	2
TPB[46]	204	91.4% after 100 cycles at 0.2C	two stages: 3.05 and 2	1−1.4
P($4VC_{86}$-*stat*-$LiSS_{14}$)[40]	360	100% after 530 cycles at 5C	3.1	0.31−1.34
poly(vinylphenothiazine)[47]	50	93% after 10000 cycles at 10C	3.5	0.07−0.37
NDI (this work, typical mass loading)	200	96% after 400 cycles at 1C 81% after 2000 cycles at 5C	2.5	1−2
NDI (this work, high mass loading)	176	164.5 mAh g^{-1} after 400 cycles at 1C	2.5	20

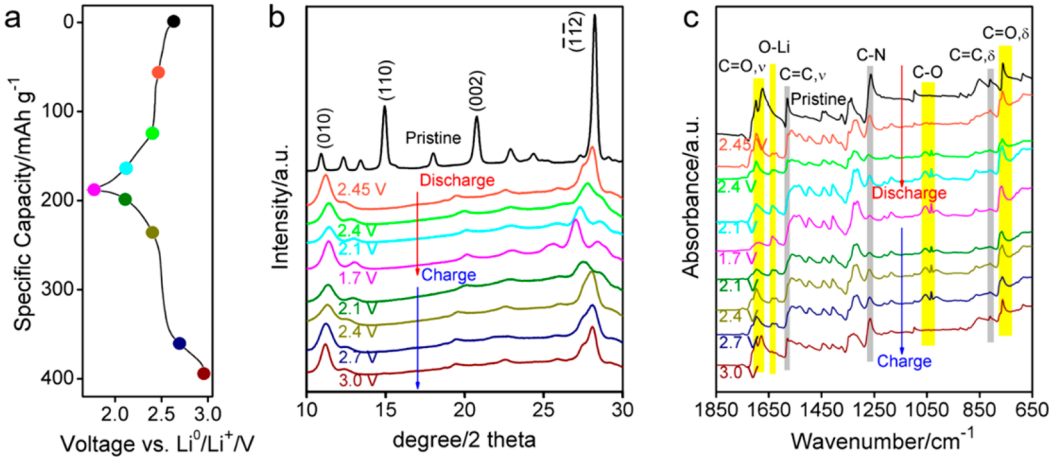

Figure 5. (a) Voltage profiles of NDI in the first discharge and charge cycle, (b) corresponding *ex-situ* XRD spectra at different states of charge, and (c) corresponding *ex-situ* FT-IR spectra at different states of charge.

NDI shows excellent reversibility in the following cycles (Figure S5). We believe that the intercalation and deintercalation of Li^+ involve multiple steps, and some intermediate phases appear during the process. Figure 4b displays the voltage profiles of NDI in the first three cycles at C/5, showing a discharge voltage plateau of 2.5 V vs Li/Li^+. The rate capability of cathode materials is related to the electron- and ion-transfer rates of the redox reaction, and many redox polymers have limited rate capabilities because of their insulating nature.[40] Our NDI electrode can deliver a discharge capacity of 190.0, 180.5, 176.9, 175.0, 172.5, 167.6, and 156.1 mAh g^{-1} at C/5, 1C, 2C, 5C, 10C, 20C, 50C, respectively (Figure 4c). The capacity retention of 82% at 50C (compared with C/5) strongly suggests its superior rate capability. This is due to the high electron mobility in its extended conjugated ring system as well as the submicrometer size feature of the particles. To further probe the electrochemical charge/discharge performance of NDI, a series of cycling tests were performed with a normal mass loading of 1−2 mg cm^{-2} to investigate the intrinsic properties of NDI. In Figure 4d, the cells were cycled in the voltage range of 1.7−3 V and 1.2−3 V at 1C, with the first three cycles at C/5 for activation. The cycling at 1.7−3 V provides a capacity of 173.5 mAh g^{-1} in the first cycle at 1C. After the initial activation cycles, the NDI electrode maintained a capacity of 177.5 mAh g^{-1} after 400 cycles. A lower cutoff voltage of 1.2 V was selected with the purpose of approaching higher capacity. It is found that a broader voltage window can indeed boost the capacity to 210.3 mAh g^{-1} in the first cycle at 1C and maintained a capacity of 201.2 mAh g^{-1} after 400 cycles, corresponding to a capacity retention of 95.7%. The relatively faster capacity degradation in the cycling with 1.2 V cutoff voltage is believed to result from the irreversible crystal structure change with a deep discharging (to be discussed later in DFT calculations). A cycling stability test was also performed at higher rates. For example, even at 5C, the capacity of NDI electrodes only degraded from the initial value of 174.9 mAh g^{-1} to 141.1 mAh g^{-1} after 2000 cycles, with a degradation rate of only 0.01% per cycle (Figure 4e). Overall, the cycling performance of NDI is comparable with or even better than some of best organic cathode materials in the literature. A summary of the organic cathode materials with the best electrochemical performance is displayed in Table 1. These materials represent the organic cathode materials with the best electrochemical performance, and compared with them, NDI shows superior electrochemical performance with a proper balance of voltage (2.5 V vs Li/Li^+), capacity (200 mAh g^{-1}), retention (81% after 2000 cycles at 5C), and rate capability (82% at 50C vs C/5).

To achieve high energy density for lithium-ion cells, high mass loading electrodes are often needed.[19,47] However, the fabrication of such electrodes is challenging because it often leads to poor cycling performance due to inferior charge transport and easy mechanical degradation.[40] High mass loading organic cathodes have been rarely reported in the literature, and the typical mass loading ranges from 0.07 to 2 mg cm^{-2} (Table 1). However, for our NDI electrodes in 1 M LiTFSI in DOL:DME electrolyte, even with a mass loading as high as 20 mg cm^{-1}, it still maintains a stable specific capacity of

DOI: 10.1021/acs.chemmater.8b01304
Chem. Mater. XXXX, XXX, XXX−XXX

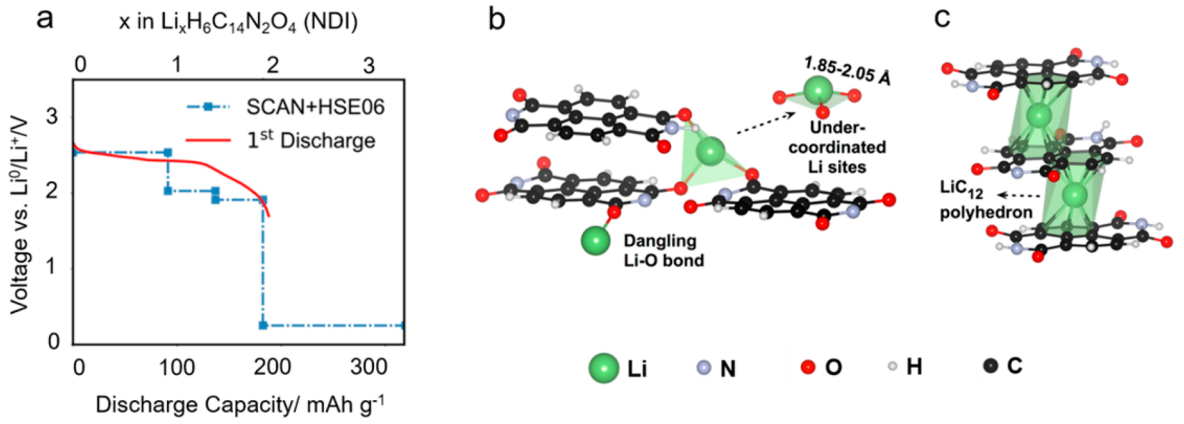

Figure 6. (a) Voltage profiles of simulated (using SCAN+HSE06 functionals) and experimental first discharge of NDI. (b) Li coordination sites in NDI molecule (2Li/NDI). (c) Extra Li coordination sites in NDI molecule (4Li/NDI).

164.5 mAh g^{-1}, corresponding to an area capacity of 3.29 mAh cm^{-2} after 400 cycles (Figure 4f). Considering the excellent cycling stability, ultrahigh rate capability, and the ability to support high mass loading electrodes, it poses great interest to fully understand the electrochemical charge/discharge process of the NDI electrodes, including the following: (1) Why is the rate capability high? (2) How does structure evolve during cycling? (3) What is the fundamental limitation for the storage capacity?

EIS measurements on NDI electrodes at different temperatures were performed, and the activation energy of the lithiation reaction was calculated to be only 0.14 eV (Figure S6). The activation energy of NDI is much smaller than those of the organic cathode materials such as polyimide (0.33 eV) and tetracyanoquinodimethane (0.53 eV)[48,49] as well as the inorganic cathode materials such as $LiCoO_2$ (0.3 eV) and $Li_{1.2}Co_{0.13}Ni_{0.13}Mn_{0.54}O_2$ (0.53 eV).[50,51] The lower activation energy correlates to faster Li^+ migration and electron-transfer rates,[52] thus explaining the superior electrochemical performance of NDI. In addition, the DFT calculated HSE band gaps for the pristine and lithiated NDI are 2.48 and 1.52 eV (Figure S7), which suggests that NDI has reasonable electronic conductivity that improves upon lithiation. This result further explains the fast electrode kinetics of the NDI electrodes.

***Ex-Situ* XRD.** To investigate the crystal structure change during the lithiation and delithiation process, *ex-situ* XRD was performed in the first discharge−charge cycle. The voltage profile in the first discharge and charge cycle is shown in Figure 5a, and the positions correspond to the samples for XRD measurement (Figure 5b). During discharging, clear changes in peak positions and intensity can be detected for (010), (110), (002), and (−1−12) planes. The (010) peak shifts to the right during discharging, which indicates decreased distance between (010) planes, while the (−1−12) peak shift to the left, which indicates increased distance between (−1−12) planes. It is noted that (−1−12) is the main plane for the layered structure, and the distance is increased due to the insertion of Li^+. (110) and (002) planes disappear during lithiation, which is believed to result from the disorder attributed to the weakened $\pi-\pi$ stacking interactions by Li^+ insertion and lowered crystallinity.[53] The disappearance of these two planes happens immediately after lithiation, which is clearly seen in the XRD pattern at 2.45 V. During charging, the distance between (−1−12) planes decreases back due to delithiation, and the distance between (010) planes increases correspondingly. The (110) and (002) planes no longer reappear, indicating an irreversible structural change in the initial cycle. As Figure 4a shows, starting from the second cycle, the cathodic peak evolves into two separate peaks and the anodic peak evolves into three separate peaks gradually, which is believed to result from the irreversible structural change. The perfectly parallel NDI molecules in their pristine state is not favorable for lithiation, and NDI molecules move and rotate to accommodate the Li^+. The fact that (110) and (002) planes no longer appear after the initial cycle favors the effective lithiation of NDI over multiple cycles, since overcoming the barrier of phase transformation in each following cycle is no longer needed.

***Ex-Situ* FT-IR.** The *ex-situ* FT-IR spectroscopy measurement was performed to identify the Li^+ coordination sites during discharging (Figure 5b). The bands at 1699 and 1673 cm^{-1} correspond to the symmetric and asymmetric C═O stretching vibrations, and the band at 761 cm^{-1} corresponds to the C═O bending vibration.[54,55] With Li^+ insertion, the C═O stretching vibrations gradually weaken, and the C═O bending vibration shifts to a higher wavenumber. The band at 1633 cm^{-1} corresponds to the lithium enolate groups (C−O−Li).[55] The spectra confirm that oxygen coordinates with Li^+ when it is inserted. There are also some reversible shifts in the absorption bands at 1578, 1264, and 809 cm^{-1}, corresponding to C═C stretching, C−N vibration, and C═C bending.[53,56] These reversible changes of the chemical environment during lithiation and delithiation also explain the good cycling stability of the NDI electrodes.

DFT Calculations. DFT calculations were performed to probe the structure and voltage profile of NDI. The starting geometry of pristine NDI was obtained from experiments, and up to four Li were inserted into the NDI structure, with distinct configurations being enumerated using the algorithm of Hart et al.[57] For both pristine and lithiated NDI, we find that the strongly constrained and appropriately normed (SCAN) meta-GGA functional[58] yields lattice parameters and XRD patterns that are in excellent agreement with experiments (Table S1 and Figure S8), outperforming even the optB88 van der Waals functional[59] and the screened hybrid Heyd−Scuseria−Ernzerhof (HSE06) functional.[60,61] This is in line with prior benchmarks of SCAN's performance on geometries of diversely bonded (e.g., ionic, covalent, hydrogen, van der Waals) materials.[62] The energies for the SCAN-relaxed structures were then computed using the HSE06 functional, which has been shown to yield much more accurate redox energies.[63]

DOI: 10.1021/acs.chemmater.8b01304
Chem. Mater. XXXX, XXX, XXX−XXX

Figure 6a shows the computed voltage profile for up to 4 Li insertion into NDI, and stable phases are observed at x = 1, 1.5, and 2. The average voltage for 2 Li insertion is in good agreement with the experimentally measured voltage. Figures 6b and 6c show the lowest energy structures for 2Li-NDI and 4Li-NDI, respectively. In 2Li-NDI, we observe that Li occupies two sites: an undercoordinated site (coordinated by three NDI molecules) and another site forming a Li−O dangling bond. In both sites, the Li−O bond distance is approximately 1.9 Å. When more than 2 Li are inserted into NDI, intercalation occurs between carbon layers, similar to graphitic anodes, forming a LiC_{12} polyhedra. This is likely the reason why intercalation of further 2 Li into the 2Li-NDI is predicted to occur at an extremely low voltage of 0.25 V vs Li/Li^+ (Figure 6a), close to the voltage for intercalation of Li into graphite (~0.2−0.3 V vs Li/Li^+).[64,65] Unlike graphite, however, 2Li-NDI has a much smaller interlayer spacing (~2.8 Å vs 3.4 Å for graphite) due to the Li−O bonding, which we hypothesize would lead to much slower kinetics for further Li insertion/extraction between the layers. This is consistent with the observed faster capacity decay with a lower cutoff voltage of 1.2 V (Figure 4d) and highlights the challenges of achieving 4 Li intercalation in NDI.

CONCLUSIONS

In summary, our study suggests that the electrode−electrolyte interaction can be the key factor determining the charge storage capacity, cycling stability, and rate capability of the organic redox electrodes. Through identifying suitable electrolytes, we were able to systematically investigate the intrinsic electrochemical reactivity of redox molecules through combined experimental characterization and DFT calculation. This leads to the rediscovery of the promising NDI electrode, which was considered to be not stable for lithium ion storage. It can achieve near theoretical lithium storage capacity and maintain high cycling stability as well as superior rate capability. This study highlights the importance of fundamental understanding on the interaction between redox molecules and electrolytes in discovering new organic electrodes.

ASSOCIATED CONTENT

Supporting Information

The Supporting Information is available free of charge on the ACS Publications website at DOI: 10.1021/acs.chemmater.8b01304.

Activation energy calculation; DFT calculations; lattice planes; solubility test; FT-IR and NMR spectra; CV plots; Nyquist plots; electronic structure (PDF)

AUTHOR INFORMATION

Corresponding Author

*(Z.C.) E-mail zhengchen@eng.ucsd.edu.

ORCID

Yang Shi: 0000-0003-2002-0343
Hanmei Tang: 0000-0003-2659-7768
Darren J. Lipomi: 0000-0002-5808-7765
Shyue Ping Ong: 0000-0001-5726-2587
Zheng Chen: 0000-0002-9186-4298

Notes

The authors declare no competing financial interest.

ACKNOWLEDGMENTS

Z.C. acknowledges the start-up fund support from Jacob School of Engineering at UC San Diego. D.J.L. acknowledges support from the Air Force Office of Scientific Research Grant FA9550-16-1-0220. H.T. and S.P.O. acknowledge funding from the U.S. Department of Energy, Office of Science, Basic Energy Sciences, under Award DE-SC0012118 for the computational portion of the work as well as computing resources provided by Triton Shared Computing Cluster (TSCC) at the UC San Diego, the National Energy Research Scientific Computing Center (NERSC), and the Extreme Science and Engineering Discovery Environment (XSEDE) supported by the National Science Foundation under Grant ACI-1053575.

REFERENCES

(1) Nayak, P. K.; Yang, L.; Brehm, W.; Adelhelm, P. From Lithium-Ion to Sodium-Ion Batteries: Advantages, Challenges, and Surprises. *Angew. Chem., Int. Ed.* **2018**, *57*, 102−120.

(2) Nitta, N.; Wu, F.; Lee, J. T.; Yushin, G. Li-Ion Battery Materials: Present and Future. *Mater. Today* **2015**, *18*, 252−264.

(3) Wu, S.; Wang, W.; Li, M.; Cao, L.; Lyu, F.; Yang, M.; Wang, Z.; Shi, Y.; Nan, B.; Yu, S.; Sun, Z.; Liu, Y.; Lu, Z. Highly Durable Organic Electrode for Sodium-Ion Batteries via a Stabilized Alpha-C Radical Intermediate. *Nat. Commun.* **2016**, *7*, 13318.

(4) Larcher, D.; Tarascon, J. M. Towards Greener and More Sustainable Batteries for Electrical Energy Storage. *Nat. Chem.* **2015**, *7*, 19−29.

(5) Liang, Y.; Tao, Z.; Chen, J. Organic Electrode Materials for Rechargeable Lithium Batteries. *Adv. Energy Mater.* **2012**, *2*, 742−769.

(6) Luo, Z.; Liu, L.; Zhao, Q.; Li, F.; Chen, J. An Insoluble Benzoquinone-Based Organic Cathode for Use in Rechargeable Lithium-Ion Batteries. *Angew. Chem., Int. Ed.* **2017**, *56*, 12561−12565.

(7) Liu, T.; Kim, K. C.; Lee, B.; Chen, Z.; Noda, S.; Jang, S. S.; Lee, S. W. Self-Polymerized Dopamine as an Organic Cathode for Li- and Na-Ion Batteries. *Energy Environ. Sci.* **2017**, *10*, 205−215.

(8) Song, Z.; Zhou, H. Towards Sustainable and Versatile Energy Storage Devices: An Overview of Organic Electrode. *Energy Environ. Sci.* **2013**, *6*, 2280−2301.

(9) Qin, H.; Song, Z. P.; Zhan, H.; Zhou, Y. H. Aqueous Rechargeable Alkali-Ion Batteries with Polyimide Anode. *J. Power Sources* **2014**, *249*, 367−372.

(10) Kim, D. J.; Je, S. H.; Sampath, S.; Choi, J. W.; Coskun, A. Effect of N-substitution in Naphthalenediimides on the Electrochemical Performance of Organic Rechargeable Batteries. *RSC Adv.* **2012**, *2*, 7968−7970.

(11) Xie, J.; Zhang, Q. Recent Progress in Rechargeable Lithium Batteries with Organic Materials as Promising Electrodes. *J. Mater. Chem. A* **2016**, *4*, 7091−7106.

(12) Shimizu, A.; Kuramoto, H.; Tsujii, Y.; Nokami, T.; Inatomi, Y.; Hojo, N.; Suzuki, H.; Yoshida, J. I. Introduction of Two Lithiooxycarbonyl Groups Enhances Cyclability of Lithium Batteries with Organic Cathode Materials. *J. Power Sources* **2014**, *260*, 211−217.

(13) Kim, H.; Kwon, J. E.; Lee, B.; Hong, J.; Lee, M.; Park, S. Y.; Kang, K. High Energy Organic Cathode for Sodium Rechargeable Batteries. *Chem. Mater.* **2015**, *27*, 7258−7264.

(14) Chen, D.; Avestro, A. J.; Chen, Z.; Sun, J.; Wang, S.; Xiao, M.; Erno, Z.; Algaradah, M. M.; Nassar, M. S.; Amine, K.; Meng, Y.; Stoddart, J. F. A Rigid Naphthalenediimide Triangle for Organic Rechargeable Lithium-Ion Batteries. *Adv. Mater.* **2015**, *27*, 2907−2912.

(15) Luo, Z.; Liu, L.; Zhao, Q.; Li, F.; Chen, J. An Insoluble Benzoquinone-Based Organic Cathode for Use in Rechargeable Lithium-Ion Batteries. *Angew. Chem., Int. Ed.* **2017**, *56*, 12561−12565.

(16) Schon, T. B.; Tilley, A. J.; Kynaston, E. L.; Seferos, D. S. Three-Dimensional Arylene Diimide Frameworks for Highly Stable Lithium Ion Batteries. *ACS Appl. Mater. Interfaces* **2017**, *9*, 15631−15637.

(17) Lakraychi, A. E.; Fahsi, K.; Aymard, L.; Poizot, P.; Dolhem, F.; Bonnet, J. P. Carboxylic and Sulfonic N-Substituted Naphthalene

DOI: 10.1021/acs.chemmater.8b01304
Chem. Mater. XXXX, XXX, XXX−XXX

Diimide Salts as Highly Stable Non-Polymeric Organic Electrodes for Lithium Batteries. *Electrochem. Commun.* **2017**, *76*, 47−50.
(18) Veerababu, M.; Kothandaraman, R. Rational Functionalization of Perylene Diimide for Stable Capacity and Long-term Cycling Performance for Li-ion Batteries. *Electrochim. Acta* **2017**, *232*, 244−253.
(19) Liang, Y.; Jing, Y.; Gheytani, S.; Lee, K. Y.; Liu, P.; Facchetti, A.; Yao, Y. Universal Quinone Electrodes for Long Cycle Life Aqueous Rechargeable Batteries. *Nat. Mater.* **2017**, *16*, 841−848.
(20) Chen, C.; Zhao, X.; Li, H. B.; Gan, F.; Zhang, J.; Dong, J.; Zhang, Q. Naphthalene-Based Polyimide Derivatives as Organic Electrode Materials for Lithium-ion Batteries. *Electrochim. Acta* **2017**, *229*, 387−395.
(21) Wurthner, F.; Stolte, M. Naphthalene and Perylene Diimides for Organic Transistors. *Chem. Commun.* **2011**, *47*, 5109−5115.
(22) Al Kobaisi, M.; Bhosale, S. V.; Latham, K.; Raynor, A. M.; Bhosale, S. V. Functional Naphthalene Diimides: Synthesis, Properties, and Applications. *Chem. Rev.* **2016**, *116*, 11685−11796.
(23) Wu, Z. H.; Huang, Z. T.; Guo, R. X.; Sun, C. L.; Chen, L. C.; Sun, B.; Shi, Z. F.; Shao, X.; Li, H.; Zhang, H. L. 4,5,9,10-Pyrene Diimides: A Family of Aromatic Diimides Exhibiting High Electron Mobility and Two-Photon Excited Emission. *Angew. Chem., Int. Ed.* **2017**, *56*, 13031−13035.
(24) Vadehra, G. S.; Maloney, R. P.; Garcia-Garibay, M. A.; Dunn, B. Naphthalene Diimide Based Materials with Adjustable Redox Potentials: Evaluation for Organic Lithium-Ion Batteries. *Chem. Mater.* **2014**, *26*, 7151−7157.
(25) Sotiriou-Leventis, C.; Mao, Z. A Facile Synthesis of 2,7-Diazapyrene. *J. Heterocycl. Chem.* **2000**, *37*, 1665−1667.
(26) Keeling, D. L.; Oxtoby, N. S.; Wilson, C.; Humphry, M. J.; Champness, N. R.; Beton, P. H. Assembly and Processing of Hydrogen Bond Induced Supramolecular Nanostructures. *Nano Lett.* **2003**, *3*, 9−12.
(27) Shi, Y.; Zhang, M.; Qian, D.; Meng, Y. S. Ultrathin Al_2O_3 Coatings for Improved Cycling Performance and Thermal Stability of $LiNi_{0.5}Co_{0.2}Mn_{0.3}O_2$ Cathode Material. *Electrochim. Acta* **2016**, *203*, 154−161.
(28) Kim, H. J.; Bae, I. S.; Cho, S. J.; Boo, J. H.; Lee, B. C.; Heo, J.; Chung, I.; Hong, B. Synthesis and Characteristics of NH_2-Functionalized Polymer Films to Align and Immobilize DNA Molecules. *Nanoscale Res. Lett.* **2012**, *7*, 30.
(29) Clark, M. B.; Gardella, J. A.; Schultz, T. M.; Patil, D. G.; Salvati, L. Solid-State Analysis of Eumelanin Biopolymers by Electron Spectroscopy for Chemical Analysis. *Anal. Chem.* **1990**, *62*, 949−956.
(30) Zangmeister, R. A.; Morris, T. A.; Tarlov, M. J. Characterization of Polydopamine Thin Films Deposited at Short Times by Autoxidation of Dopamine. *Langmuir* **2013**, *29*, 8619−8628.
(31) Wu, M. X.; Feng, Q. B.; Sun, X.; Wang, H. L.; Gielen, G.; Wu, W. X. Rice (Oryza Sativa L) Plantation Affects the Stability of Biochar in Paddy Soil. *Sci. Rep.* **2015**, *5*, 10001.
(32) Liang, Y.; Zhang, P.; Chen, J. Function-Oriented Design of Conjugated Carbonyl Compound Electrodes for High Energy Lithium Batteries. *Chem. Science.* **2013**, *4*, 1330−1337.
(33) Yanagi, K.; Akiyoshi, S. Hydroxyethylation of Imides. *J. Org. Chem.* **1959**, *24*, 1122−1123.
(34) Zarzyka-Niemiec, I. Reactions of Oxamide with Ethylene Carbonate. *Polimery* **2011**, *56*, 196−203.
(35) Zarzyka-Niemiec, I. Polyhydroxyalkylation of Urea with Ethylene Carbonate and Application of Obtained Products as Components of Polyurethane Foams. *e-Polym.* **2008**, *8*, 1−15.
(36) Zarzyka, I.; Łukasiewicz-Czul, B.; Pacześniak, T.; Stagraczyński, R.; Majda, D. Effect of the Additive Fire Retardants on the Properties of Rigid Polyurethane Foams, Obtained Using Hydroxyethyl Derivatives of Oxamide and Polymeric 4,4'-diphenylmethane Diisocyanate. *Polym.-Plast. Technol. Eng.* **2015**, *54*, 1280−1288.
(37) Lubczak, R.; Duliban, J. A Study of the Reaction of Adenine with Ethylene Oxide or with Ethylene Carbonate. *React. Funct. Polym.* **2002**, *52*, 127−134.
(38) Ustyuzhanin, G. E.; Kolomeitseva, V. V.; Tikhomirova-Sidorova, N. S. Hydroxyethylation of Uracil, Adenine, and Cytosine with Ethylene Carbonate. *Chem. Heterocycl. Compd.* **1978**, *14*, 562−566.
(39) Eissa, A. G.; Blaxland, J. A.; Williams, R. O.; Metwally, K. A.; El-Adl, S. M.; Lashine, E. S. M.; Baillie, L. W. J.; Simons, C. Adenine and Benzimidazole-Based Mimics of REP-3123 as Antibacterial Agents against Clostridium Difficile and Bacillus Anthracis: Design, Synthesis and Biological Evaluation. *Bull. Fac. Pharm.* **2016**, *54*, 197−207.
(40) Kolek, M.; Otteny, F.; Schmidt, P.; Muck-Lichtenfeld, C.; Einholz, C.; Becking, J.; Schleicher, E.; Winter, M.; Bieker, P.; Esser, B. Ultra-High Cycling Stability of Poly(vinylphenothiazine) as a Battery Cathode Material Resulting from $\pi-\pi$ Interactions. *Energy Environ. Sci.* **2017**, *10*, 2334−2341.
(41) Nokami, T.; Matsuo, T.; Inatomi, Y.; Hojo, N.; Tsukagoshi, T.; Yoshizawa, H.; Shimizu, A.; Kuramoto, H.; Komae, K.; Tsuyama, H.; Yoshida, J. I. Polymer-Bound Pyrene-4,5,9,10-tetraone for Fast-Charge and -Discharge Lithium-Ion Batteries with High Capacity. *J. Am. Chem. Soc.* **2012**, *134*, 19694−19700.
(42) Lee, M.; Hong, J.; Kim, H.; Lim, H. D.; Cho, S. B.; Kang, K.; Park, C. B. Organic Nanohybrids for Fast and Sustainable Energy Storage. *Adv. Mater.* **2014**, *26*, 2558−2565.
(43) Zhang, K.; Guo, C.; Zhao, Q.; Niu, Z.; Chen, J. High-Performance Organic Lithium Batteries with an Ether-Based Electrolyte and 9,10-Anthraquinone (AQ)/CMK-3 Cathode. *Adv. Sci.* **2015**, *2*, 1500018.
(44) Song, Z.; Qian, Y.; Gordin, M. L.; Tang, D.; Xu, T.; Otani, M.; Zhan, H.; Zhou, H.; Wang, D. Polyanthraquinone as a Reliable Organic Electrode for Stable and Fast Lithium Storage. *Angew. Chem., Int. Ed.* **2015**, *54*, 13947−13951.
(45) Song, Z.; Qian, Y.; Liu, X.; Zhang, T.; Zhu, Y.; Yu, H.; Otani, M.; Zhou, H. A Quinone-Based Oligomeric Lithium Salt for Superior Li-Organic Batteries. *Energy Environ. Sci.* **2014**, *7*, 4077−4086.
(46) Patil, N.; Aqil, A.; Ouhib, F.; Admassie, S.; Inganäs, O.; Jérôme, C.; Detrembleur, C. Bioinspired Redox-Active Catechol-Bearing Polymers as Ultrarobust Organic Cathodes for Lithium Storage. *Adv. Mater.* **2017**, *29*, 1703373.
(47) Lee, M.; Hong, J.; Lopez, J.; Sun, Y.; Feng, D.; Lim, K.; Chueh, W. C.; Toney, M. F.; Cui, Y.; Bao, Z. High-Performance Sodium-Organic Battery by Realizing Four-Sodium Storage in Disodium Rhodizonate. *Nat. Energy* **2017**, *2*, 861−868.
(48) Aziz, N. D. A.; Kamarulzaman, N.; Subban, R. H. Y.; Hamzah, A. S.; Ahmed, A. Z.; Osman, Z.; Rusdi, R.; Kamarudin, N.; Mohalid, N.; Romli, A. Z.; Shaameri, Z. The Electrical Conductivities of Polyimide and Polyimide/Li Triflate Composites: An a.c. Impedance Study. *AIP Conf. Proc.* **2017**, *1877*, 060007.
(49) Chen, Y.; Sun, S.; Wang, X.; Shi, Q. Study of Lithium Migration Pathways in the Organic Electrode Materials of Li-Battery by Dispersion-Corrected Density Functional Theory. *J. Phys. Chem. C* **2015**, *119*, 25719−25725.
(50) Yang, S.; Yan, B.; Wu, J.; Lu, L.; Zeng, K. Temperature-Dependent Lithium-Ion Diffusion and Activation Energy of $Li_{1.2}Co_{0.13}Ni_{0.13}Mn_{0.54}O_2$ Thin-Film Cathode at Nanoscale by Using Electrochemical Strain Microscopy. *ACS Appl. Mater. Interfaces* **2017**, *9*, 13999−14005.
(51) Nakamura, K.; Ohno, H.; Okamura, K.; Michihiro, Y.; Moriga, T.; Nakabayashi, I.; Kanashiro, T. Li-7 NMR Study on Li^+ Ionic Diffusion and Phase Transition in Li_xCoO_2. *Solid State Ionics* **2006**, *177*, 821−826.
(52) Okubo, M.; Tanaka, Y.; Zhou, H.; Kudo, T.; Honma, I. Determination of Activation Energy for Li Ion Diffusion in Electrodes. *J. Phys. Chem. B* **2009**, *113*, 2840−2847.
(53) Kim, D. J.; Jung, Y. H.; Bharathi, K. K.; Je, S. H.; Kim, D. K.; Coskun, A.; Choi, J. W. An Aqueous Sodium Ion Hybrid Battery Incorporating an Organic Compound and a Prussian Blue Derivative. *Adv. Energy Mater.* **2014**, *4*, 1400133.
(54) Kar, H.; Gehrig, D. W.; Allampally, N. K.; Fernandez, G.; Laquai, F.; Ghosh, S. Cooperative Supramolecular Polymerization of An Amine-Substituted Naphthalene-Diimide and Its Impact on

DOI: 10.1021/acs.chemmater.8b01304
Chem. Mater. XXXX, XXX, XXX−XXX

Excited State Photophysical Properties. *Chem. Sci.* **2016**, *7*, 1115−1120.
(55) Luo, W.; Allen, M.; Raju, V.; Ji, X. An Organic Pigment as a High-Performance Cathode for Sodium-Ion Batteries. *Adv. Energy Mater.* **2014**, *4*, 1400554.
(56) Schon, T. B.; Tilley, A. J.; Kynaston, E. L.; Seferos, D. S. Three-Dimensional Arylene Diimide Frameworks for Highly Stable Lithium Ion Batteries. *ACS Appl. Mater. Interfaces* **2017**, *9*, 15631−15637.
(57) Hart, G. L. W.; Forcade, R. W. Algorithm for Generating Derivative Structures. *Phys. Rev. B: Condens. Matter Mater. Phys.* **2008**, *77*, 224115.
(58) Sun, J.; Ruzsinszky, A.; Perdew, J. P. Strongly Constrained and Appropriately Normed Semilocal Density Functional. *Phys. Rev. Lett.* **2015**, *115*, 036402.
(59) Klimeš, J.; Bowler, D. R.; Michaelides, A. Van der Waals Density Functionals Applied to Solids. *Phys. Rev. B: Condens. Matter Mater. Phys.* **2011**, *83*, 195131.
(60) Heyd, J.; Scuseria, G. E.; Ernzerhof, M. Hybrid Functionals Based on a Screened Coulomb Potential. *J. Chem. Phys.* **2003**, *118*, 8207−8215.
(61) Heyd, J.; Scuseria, G. E.; Ernzerhof, M. Erratum: "Hybrid Functionals Based on A Screened Coulomb Potential. *J. Chem. Phys.* **2006**, *124*, 219906.
(62) Sun, J.; Remsing, R. C.; Zhang, Y.; Sun, Z.; Ruzsinszky, A.; Peng, H.; Yang, Z.; Paul, A.; Waghmare, U.; Wu, X.; Klein, M. L.; Perdew, J. P. Accurate First-Principles Structures and Energies of Diversely Bonded Systems from An Efficient Density Functional. *Nat. Chem.* **2016**, *8*, 831−836.
(63) Chevrier, V. L.; Ong, S. P.; Armiento, R.; Chan, M. K. Y.; Ceder, G. Hybrid Density Functional Calculations of Redox Potentials and Formation Energies of Transition Metal Compounds. *Phys. Rev. B: Condens. Matter Mater. Phys.* **2010**, *82*, 075122.
(64) Shu, Z. X.; McMillan, R. S.; Murray, J. J. Electrochemical Intercalation of Lithium into Graphite. *J. Electrochem. Soc.* **1993**, *140*, 922−927.
(65) Dahn, J. R. Phase Diagram of Li_xC_6. *Phys. Rev. B: Condens. Matter Mater. Phys.* **1991**, *44*, 9170−9177.

DOI: 10.1021/acs.chemmater.8b01304
Chem. Mater. XXXX, XXX, XXX−XXX